npj | climate and atmospheric science

www.nature.com/npjclimatsci

ARTICLE OPEN

Check for updates

Important role of stratosphere-troposphere coupling in the Arctic mid-to-upper tropospheric warming in response to sea-ice loss

Mian Xu[1], Wenshou Tian[1]✉, Jiankai Zhang[1]✉, James A. Screen[2], Chongyang Zhang[1] and Zhe Wang[1]

Recent studies have suggested that deep Arctic warming, extending from the surface to the upper troposphere, could trigger mid-latitude atmospheric circulation changes, while shallow Arctic warming, confined in the lowermost troposphere, induces comparatively weak remote responses. The causes of Arctic mid-to-upper tropospheric warming are less clear compared with near-surface warming. Here, we demonstrate a new dynamical mechanism responsible for the polar mid-to-upper tropospheric warming associated with Arctic sea-ice loss, using both reanalysis and model simulations. The Barents-Kara sea-ice loss enhances the upward propagating waves, leading to the wave convergence anomalies in the sub-polar lower stratosphere and upper troposphere. The consequent eddy feedback leads to clockwise residual overturning anomalies in the sub-polar upper and middle troposphere, accompanied by anomalous descent and consequent adiabatic warming in the Arctic mid-to-upper troposphere. The essential role of stratosphere-troposphere coupling for deep Arctic warming induced by sea-ice loss is confirmed by model simulations with stratospheric variability suppressed, in which only the Arctic lower troposphere is warmed in response to sea-ice loss. Our results suggest that a considerable part of the observed Arctic mid-to-upper warming is caused by a dynamical response to sea-ice loss, in which stratosphere-troposphere coupling plays a major role.

npj Climate and Atmospheric Science (2023)6:9; https://doi.org/10.1038/s41612-023-00333-2

INTRODUCTION

In the past 40 years, Arctic surface air temperature has risen at 3–4 times the rate of the global average[1–4]. The so-called "Arctic amplification" phenomenon has drawn much attention from scientific community, not only because of the dramatic environmental changes induced in the Arctic, but also due to the potential remote effects on the Northern Hemispheric mid-latitude weather and climate[1,5–9]. The possible remote impacts of Arctic amplification and the mechanisms responsible are poorly known[1,10,11]. Among these uncertainties is the importance of the vertical extent of Arctic warming for the potential remote responses. Some studies found that instead of surface air temperature, the atmospheric thickness between middle and lower troposphere over the Arctic region is more related to the mid-latitude atmospheric circulation[6,12]. More specifically, recent studies have suggested that deep Arctic warming, extending from the surface to the upper troposphere, may induce the changes in the Northern Hemispheric mid-latitude weather and climate, but shallow Arctic warming, confined in the lowermost troposphere, induces comparatively weak remote responses. Using a simplified model, Sellevold et al.[13] found that the Arctic warming penetrating to the upper troposphere, namely deep warming, could induce a mid-latitude circulation response, whereas Arctic near-surface warming, namely shallow warming, cannot. Previous studies[14–16] found that winter cooling anomaly over the mid-latitude Eurasia is correlated with Arctic deep warming rather than shallow warming, suggesting deep warming may be a necessary condition to induce the "warm Arctic, cold Eurasia" pattern[17–19]. This interpretation is supported by the model experiments in Labe et al.[20], which suggested a greater magnitude of circulation and Eurasian cooling response to deep Arctic warming compared with shallow Arctic warming.

The possible causes of the Arctic near-surface warming can be broadly characterized into local and remote factors[10]. Local feedbacks, such as albedo feedback[3,21–24], long-wave cloud feedback[25] and lapse rate feedback[26,27], are known to enhance Arctic warming, with the greatest warming near the surface. Remote factors, such as the poleward transport of heat and moisture through atmospheric circulation and oceanic currents[28–31], are also important and may be associated with warming aloft as well in the lowermost troposphere. Compared with the warming in the lower troposphere, the factors responsible for the Arctic mid-to-upper tropospheric warming are not yet clear, especially what component of Arctic warming aloft may be related to sea-ice loss. Cohen et al.[10] proposed that the Arctic warming aloft is mainly due to the vertical diffusion of near-surface heating caused by sea-ice loss; they speculated that this vertical mixing is underestimated by atmospheric models, leading to the warming being confined in the lowermost troposphere. Deser et al.[32] suggested the Arctic warming aloft in response to sea-ice loss is amplified by ocean-atmosphere coupling. Screen and Francis[31] found that the phase of the Pacific Decadal Oscillation could modulate the vertical extent of tropospheric warming induced by sea-ice loss through influencing the poleward advection of warm and moist air. However, He et al.[14] and Labe et al.[20] argued that internal variability, rather than Arctic sea-ice loss, is the major cause of the Arctic mid-to-upper tropospheric warming. Therefore, there remains much debate on the contribution of sea-ice loss to the Arctic mid-to-upper tropospheric warming and the mechanisms involved, which deserve further investigation.

[1]College of Atmospheric Sciences, Lanzhou University, Lanzhou, China. [2]Department of Mathematics and Statistics, University of Exeter, Exeter, UK. ✉email: wstian@lzu.edu.cn; jkzhang@lzu.edu.cn

It has been proposed that Arctic sea-ice loss, particularly in the Barents-Kara Sea (hereafter BKS), enhances the upward propagation of wave activity and thereby weakens the stratospheric polar vortex[33–35]. Then, the consequent stratospheric anomalies may descend back to the troposphere and further influence the tropospheric circulation[36–44]. However, what the specific role such stratosphere-troposphere dynamical coupling processes in response to sea-ice loss play in driving Arctic mid-to-upper tropospheric warming has been rarely discussed. Here, we demonstrate a key role of stratosphere-troposphere dynamical coupling in the Arctic warming aloft induced by the BKS sea-ice loss through observational analysis and numerical experiments, which could help improve our understanding of the role of sea-ice loss in the Arctic-mid-latitude connection.

RESULTS

Causal linkage between sea-ice loss and Arctic deep warming

Figure 1a shows the regression map of wintertime zonal-mean temperature against BKS sea-ice derived from ERA-5 reanalysis data. Over the Arctic, reduced sea ice is coincident with warming anomalies throughout the troposphere, which is of the greatest magnitude near the surface and in the upper troposphere. This warming pattern agrees well with the observed trends over recent decades[10]. Also, it is worth noting that the cooling anomaly over the mid-latitudes accompanied by deep Arctic warming (Fig. 1a) is consistent with many previous studies[13,14,20]. To clarify the causality between the Arctic sea-ice loss and deep Arctic warming, we investigate the results from PAMIP multi-model large ensemble mean and WACCM-SC simulations. In these simulations, sea ice conditions are changed whilst all other boundary and external forcings are fixed, to isolate the atmospheric response to sea-ice loss, whereas observation results could imply both the signals from the sea-ice loss and many other forcings (e.g., greenhouse gas, tropical sea surface temperature and etc.). Supplementary Figure 1 shows the wintertime zonal-mean temperature response to the future BKS sea-ice loss from all eight different models in the PAMIP project. It can be found that the results from six of these PAMIP models show deep Arctic warming, albeit not always statistically significant throughout the troposphere. However, given the low signal-to-noise ratio[45–48], we should avoid over-interpreting the individual model results, particularly from the smaller ensembles. The PAMIP multi-model ensemble mean, which could provide a more robust estimation of the forced response, shows statistically significant deep Arctic warming in response to the future BKS sea-ice loss (Fig. 1b), with a highly similar warming pattern to that found in the reanalysis, yet with a weaker magnitude (Fig. 1a). Therefore, the results from reanalysis and PAMIP multi-model mean consistently suggest that the BKS sea-ice loss is closely linked to the deep Arctic warming, which is not restricted to the lowermost troposphere. The temperature response from the free-running WACCM-SC simulations (Fig. 1c) also resembles those derived from reanalysis and PAMIP multi-model ensemble mean, with deep Arctic warming throughout the troposphere, but again of lesser magnitude in the model than reanalysis. It is important to emphasize that the simulated Arctic mid-to-upper tropospheric warming (north of 65°N, between 600 and 225 hPa) induced by sea-ice loss is only ~20% of that of the composite results from reanalysis (noting the PAMIP results have been multiplied by the ratio of the observed BKS SIC against the PAMIP forcing for a better comparison). This implies that Arctic sea-ice loss is only responsible for around one fifth of the deep Arctic warming, while the rest could be due to other factors (like ENSO) and atmospheric internal variability[14,20]. To investigate the potential role of stratosphere-troposphere coupling in the deep Arctic warming induced by sea-ice loss, the polar stratospheric variability in the WACCM-SC model is suppressed using a nudging technique (see "Methods"). The temperature response when the stratosphere-troposphere coupling is suppressed is shown in Fig. 1d. Whilst there is still significant warming anomaly in the Arctic lower troposphere, likely in response to surface heating from enhanced upward heat fluxes[3,23,24,29,49,50], the Arctic warming aloft is missing. Instead, the polar mid-to-upper troposphere cools in the absence of an interactive stratosphere. Moreover, the above-mentioned nudging results could also be implicitly validated using free-running experiments. Using wintertime 50 hPa temperature averaged north of 66°N to depict the Arctic stratospheric polar vortex strength, a year when the polar vortex strength falls within ±0.5 time standard deviation of CTRL run is defined as an inactive-polar-vortex year, while the year with the polar vortex strength larger (smaller) than +0.5 (−0.5) time standard deviation is defined as an active-polar-vortex year. Supplementary Figure 2a, b show the differences of wintertime zonal-mean temperature between LICE and HICE runs in inactive-polar-vortex and active-polar-vortex years, respectively. Note that the Arctic warming induced by sea-ice loss in inactive-polar-vortex years is confined in the polar lower troposphere, which is consistent with Fig. 1d, while the result of active-polar-vortex years shows a statistically significant pattern of Arctic deep warming (similar to Fig. 1c). Therefore, this validates our nudging results and also highlights the importance of stratosphere-troposphere coupling in the vertical extension of Arctic warming induced by sea-ice loss.

The temperature tendency equation in the Transformed Eulerian Mean (TEM) framework[51] is applied to quantify the relative contribution of the adiabatic temperature change due to vertical motion and diabatic processes to the Arctic mid-to-upper tropospheric warming induced by sea-ice loss (see "Methods"). Compared with the conventional Eulerian Mean framework, the TEM framework focuses on the influence of eddy feedback, which is more suitable for analyzing the extra-tropical atmospheric circulation[48]. The diabatic heating rate (e.g., sensible/latent heating, radiation and etc.) is directly output by WACCM model, while this variable is currently inaccessible from ERA-5 reanalysis and therefore, not shown in this study. Figure 2 shows the wintertime temperature tendency differences, between BKS low- and high-SIC scenarios and averaged in the Arctic mid-to-upper troposphere contributed by adiabatic and diabatic processes. It can be found both in reanalysis and model simulations that adiabatic heating due to anomalous descent in response to BKS sea-ice loss is favorable for the Arctic mid-to-upper tropospheric warming anomalies. Moreover, it is worth noting that the warming tendency anomaly contributed by adiabatic processes in reanalysis is around 5 times that derived from WACCM simulations, very close to the difference in warming magnitude between reanalysis and simulations from Fig. 1. Further, simulation results show that the temperature tendency anomaly contributed by diabatic processes is relatively weaker compared with that contributed by adiabatic processes. This could be due to that most of diabatic processes associated with sea-ice loss, like sensible and latent heat processes, are mainly confined in the lower troposphere[49,50,52]. However, when suppressing the stratosphere-troposphere coupling, the Arctic mid-to-upper troposphere shows anomalous cooling in response to sea-ice loss, which is mainly contributed by the adiabatic cooling due to anomalous ascent. This is consistent with the cold anomalies in the Arctic mid-to-upper troposphere found in the nudged results (Fig. 1d). In summary, adiabatic heating due to anomalous descent plays a critical role in the Arctic mid-to-upper tropospheric warming anomalies induced by sea-ice loss and the stratosphere-troposphere coupling is essential in the entire process. The underlying dynamical mechanism is further investigated in the following section.

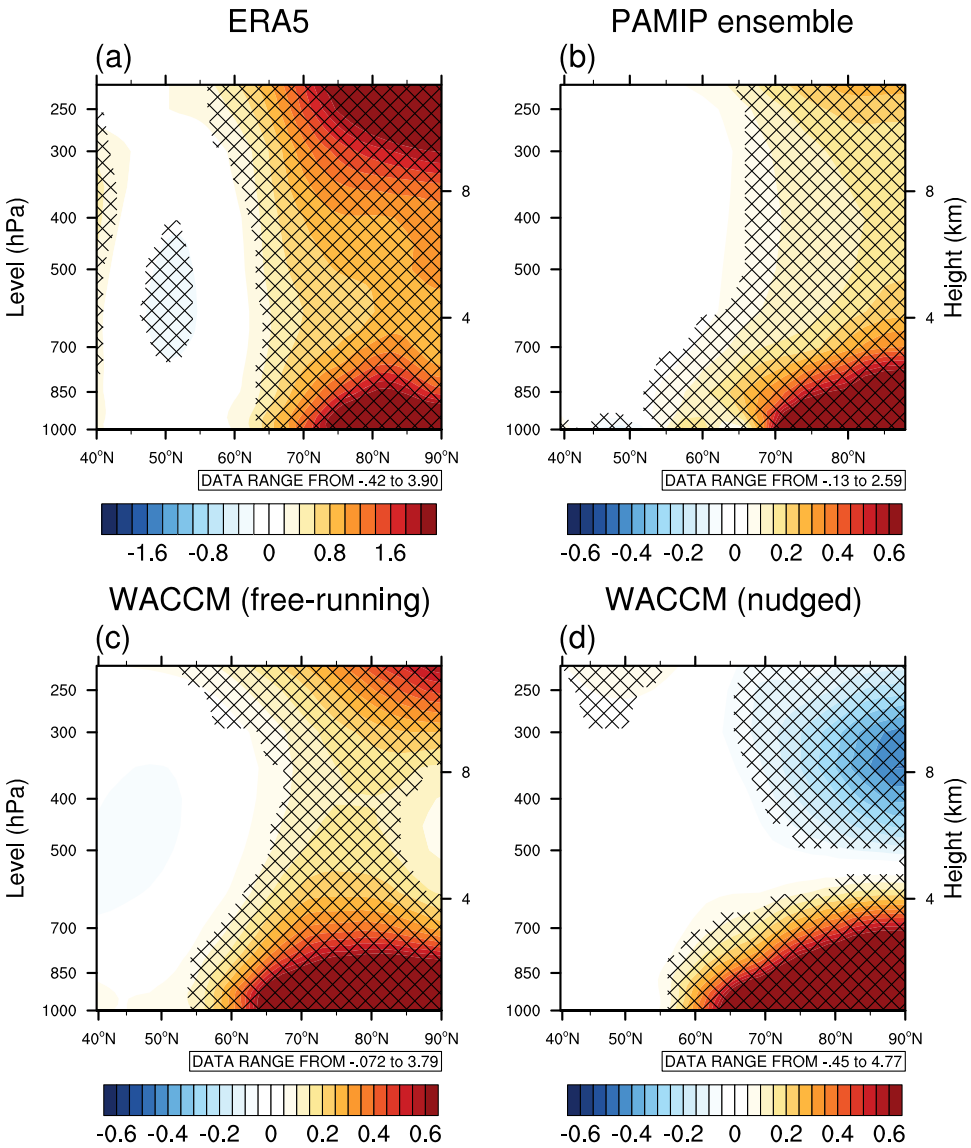

Fig. 1 Zonal-mean winter temperature anomalies induced by BKS sea-ice loss. a Zonal-mean winter temperature (K) regressed against BKS sea ice, multiplied by the composited SIC differences between BKS low- and high-SIC years, derived from the ERA5 reanalysis. Simulated zonal-mean winter temperature differences in the (**b**) PAMIP multi-model large ensemble results between pdSST-futBKSeasSIC and pdSST-pdSIC runs (multiplied by the ratio of the observed BKS SIC index differences between low- and high-SIC years against the PAMIP forcing), **c** free-running WACCM-SC simulations, and **d** nudged WACCM-SC simulations between LICE and HICE runs. The information of data range is placed above label bar. Hatched regions are statistically significant at the 90% confidence level according to bootstrap resampling statistical test.

Mechanisms and role of stratosphere-troposphere coupling

Many previous studies have revealed that the weakening of stratospheric polar vortex by enhanced upward propagating waves due to sea-ice loss could subsequently influence the tropospheric circulation through downward coupling[9,33–44]. Supplementary Figures 3a, b show the differences of E-P flux and divergence between BKS low- and high-SIC scenarios, derived from ERA-5 reanalysis and WACCM simulations. Consistent with many previous studies[36–44], the poleward and upward propagating waves are enhanced in response to sea-ice loss, leading to the wave convergence anomalies in the polar stratosphere and a weakening of stratospheric polar vortex (Supplementary Figs. 4 and 5). The deceleration of the sub-polar westerly jet further descends from the lower stratosphere to the surface, both found in reanalysis and model simulations (Supplementary Fig. 4a–c). When the stratospheric pathway is blocked in WACCM-SC model, there is only a weak easterly anomaly in the troposphere (Supplementary Fig. 4d). According to the linear theory[51], the deceleration of tropospheric westerly is favorable for the breaking of the poleward propagating eddies at a lower latitude when reaching the critical line[53,54]. Hence, there are also E-P flux convergence anomalies in the sub-polar mid-to-upper troposphere. In the nudged results, the upper tropospheric convergence anomalies are shifted poleward due to a weaker tropospheric easterly anomaly, favorable for the northward shift of wave breaking zone[54], compared with the results of free-running simulations.

To explain the adiabatic heating due to anomalous descent in the Arctic mid-to-upper troposphere, we next consider the response of the residual stream function associated with sea-ice loss. From the TEM perspective, the climatology of Northern Hemispheric mid-latitude region is dominated by a clockwise meridional overturning cell during winter in reanalysis data and model simulations (purple contours in Fig. 3a, b), consistent with Schubert et al.[55]. In response to BKS sea-ice loss, there are positive anomalies in residual stream function in the sub-polar lower

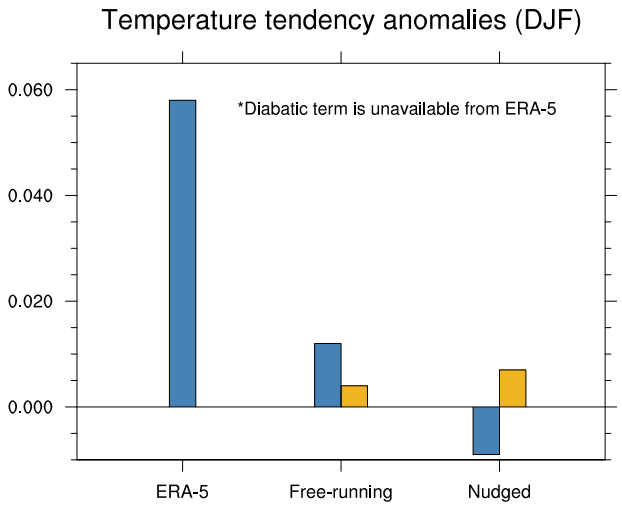

Fig. 2 Decomposition of temperature tendency anomalies in the Arctic mid-to-upper troposphere induced by BKS sea-ice loss. Bar plot of temperature tendency differences (K day^{-1}) averaged in winter (DJF) contributed by adiabatic heating/cooling due to residual vertical motion (blue) and diabatic processes (yellow) between BKS low- and high-SIC scenarios, averaged north of 65°N in mid-to-upper troposphere (600–225 hPa), derived from ERA-5 reanalysis, WACCM-SC simulations without and with nudging technique applied.

stratosphere and middle troposphere, corresponding to enhanced clockwise meridional overturning cell (Fig. 3a, b). By contrast, there are counterclockwise overturning anomalies in the sub-polar near-surface. It is worth noting that this pattern of stream function anomalies is consistent with the E-P flux convergence anomalies in the sub-polar lower stratosphere and upper troposphere associated with sea-ice loss (Supplementary Fig. 3a, b). This is because the residual stream function is inversely proportional to the vertical gradient of E-P flux divergence (see Eq. 8 in the "Methods" section). However, when the stratosphere-troposphere coupling is suppressed in the model, the E-P flux convergence anomalies in the lower stratosphere are missing in the nudged simulations. Correspondingly, the vertical gradient anomaly of eddy divergence near the sub-polar tropopause turns from negative to positive, leading to the local counterclockwise residual overturning in the lower stratosphere (Fig. 3c). In addition, the stratosphere-troposphere dynamical response to sea-ice loss can also strengthen the clockwise residual overturning anomalies in the sub-polar troposphere (Fig. 3d).

Figure 4a, b show the differences of residual vertical velocity during winter between the BKS low- and high-SIC scenarios derived from reanalysis and model simulations, respectively. It can be found that there are negative residual vertical velocity anomalies on the poleward flank of the above-mention clockwise residual overturning anomalies in the Arctic upper troposphere and lower stratosphere. The anomalous descent is responsible for the adiabatic heating in the Arctic mid-to-upper troposphere (Fig. 2). By contrast, in the nudged experiments there is anomalous ascent in the Arctic upper troposphere, leading to the adiabatic cooling and hence, the anomalous cooling found in Fig. 1d.

DISCUSSION

The potential impacts of the Arctic sea-ice loss on the Northern Hemispheric mid-latitude weather and climate have drawn much attention from the scientific community in the past few decades. However, there are many unresolved questions. One open question is whether Arctic warming needs to penetrate into the mid-troposphere to be able to influence the mid-latitude atmospheric circulation.

Recent studies have proposed that the vertical extension of Arctic warming, so-called deep Arctic warming, is key for triggering remote responses[14,20]. Based on their studies, our study further presents a new perspective on the connection between Arctic sea-ice loss and this deep Arctic warming. We found that the BKS sea-ice loss could contribute to a considerable part of the observed Arctic warming aloft mainly through modulating the stratosphere-troposphere dynamical coupling. In other words, we argue that distinct mechanisms govern the Arctic near-surface and mid-to-upper tropospheric warming induced by sea-ice loss. Considering the key role of the deep Arctic warming in the Arctic-mid-latitude connection, our work could offer a deeper insight into the potential influence of Arctic sea-ice loss on this connection. However, we have only considered the atmospheric response to Arctic sea-ice loss, which appears to explain around 20% of the observed Arctic mid-to-upper tropospheric warming. Therefore, the relative importance among Arctic sea-ice loss and many other potential factors are worth further investigation in the future. Moreover, another open question is whether Arctic mid-to-upper tropospheric warming driven by processes besides sea-ice loss is important in governing the mid-latitude climate response to Arctic amplification.

METHODS

Definitions

The BKS region is defined as the area 65°–85°N, 20°E–90°E and the BKS sea-ice concentration (SIC) index used in this study is defined as the early-winter (November and December) area-averaged SIC over the BKS region. BKS high- and low-SIC years are selected based on HadISST dataset, using the following method. First, the early winter BKS SIC time series from 1979 to 2020 was linearly detrended and then, a 1 standard deviation (std) threshold was used to identify years of high and low BKS SIC (Supplementary Fig. 6b). According to these selection criteria, 8 years were selected with high BKS SIC (1988, 1997, 1998, 2002, 2003, 2010, 2014, and 2019) and 4 years with low BKS SIC (1984, 2012, 2016, and 2020). Linear regression is applied in this study by regressing the atmospheric fields upon the above-mentioned BKS SIC time series to roughly separate the atmospheric anomalies associated with BKS sea-ice variability. Then, the obtained regression map is further multiplied by the composited BKS SIC differences between the above-mentioned BKS low- and high-SIC years (low-SIC minus high-SIC), in order to retrieve the atmospheric anomalies associated with 2-std sea-ice loss.

The Eliassen-Palm flux (E-P flux)[56] and the TEM circulation[51] are applied in this study to diagnose the response of wave activity to the BKS sea-ice loss and the effect of the consequent eddy feedback on the extra-tropical atmospheric circulation. The meridional and vertical components of the EP-flux, its divergence and the residual meridional and vertical velocity are calculated according to the following equations:

$$F_\phi = \rho a\ \cos\ \phi\left(\overline{u_z}\ \overline{v'\theta'}/\overline{\theta_z} - \overline{v'u'}\right) \tag{1}$$

$$F_z = \rho a \cos\phi\left\{\left[f - (a\cos\phi)^{-1}(\overline{u}\cos\phi)_\phi\ \overline{v'\theta'}/\overline{\theta_z} - \overline{w'u'}\right]\right\} \tag{2}$$

$$D_F = \frac{\nabla\cdot\mathbf{F}}{\rho a\cos\phi} = \frac{(a\cos\phi)^{-1}\frac{\partial}{\partial\phi}\left(F_\phi\cos\phi\right) + \frac{\partial F_z}{\partial z}}{\rho a\cos\phi} \tag{3}$$

$$\overline{v}^* = \overline{v} - \frac{\partial}{\partial p}\left(\frac{\overline{v'\theta'}}{\partial\overline{\theta}/\partial p}\right) \tag{4}$$

$$\overline{w}^* = \overline{w} + \frac{1}{a\cos\phi}\frac{\partial}{\partial\phi}\left(\frac{\overline{v'\theta'}\cos\phi}{\partial\overline{\theta}/\partial p}\right) \tag{5}$$

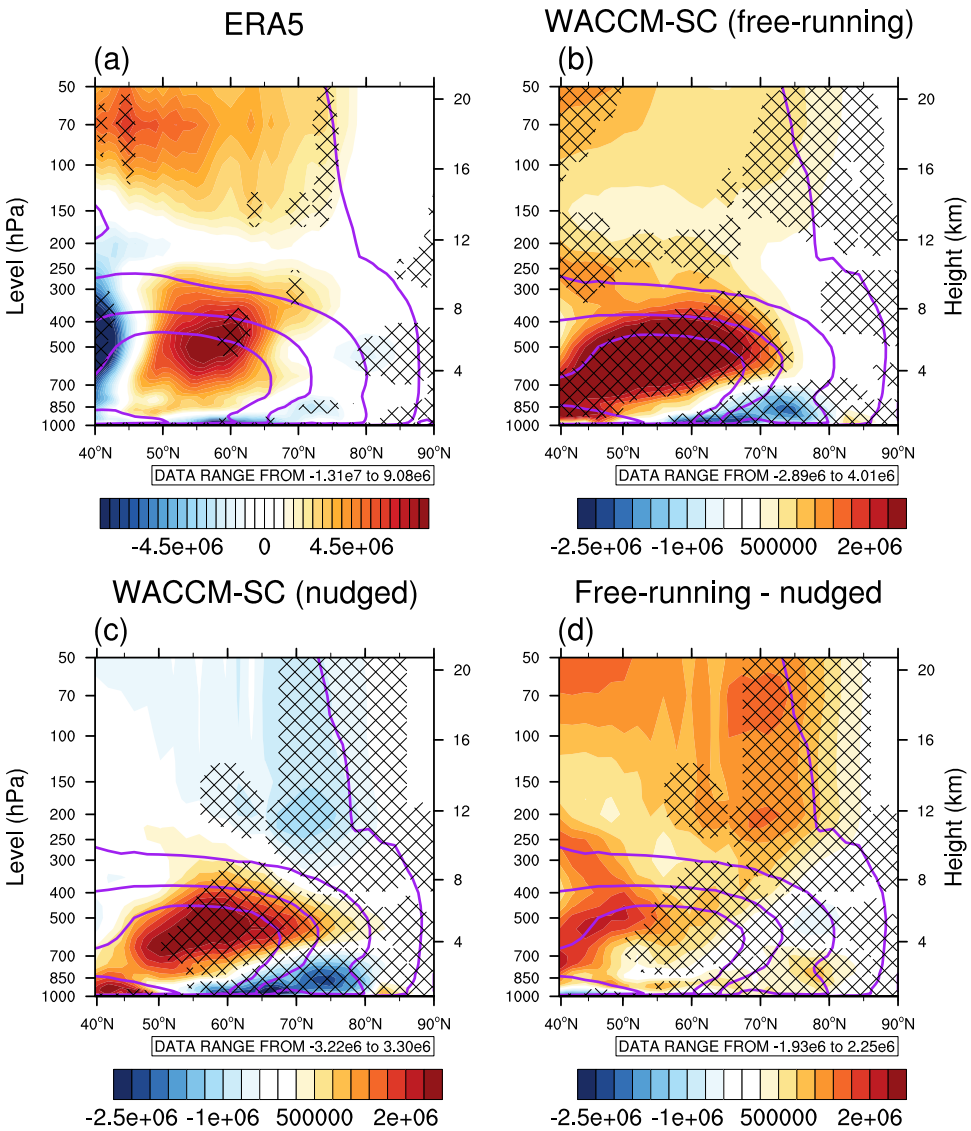

Fig. 3 Winter residual stream function anomalies induced by BKS sea-ice loss. a Zonal-mean winter residual meridional stream function (kg m^{-1} s^{-1}; scaled by air pressure) regressed against BKS sea ice, multiplied by the composited SIC differences between BKS low- and high-SIC years, derived from the ERA5 reanalysis. Simulated differences of zonal-mean winter residual meridional stream function between LICE and HICE runs in the **b** free-running WACCM-SC simulations, **c** nudged WACCM-SC simulations, and **d** their differences (free-running minus nudged). Purple contours denote the climatological state of residual meridional stream function for ERA-5 reanalysis and WACCM-SC simulations. The information of data range is placed above label bar. Hatched regions are statistically significant at the 90% confidence level according to bootstrap resampling statistical test.

where u, v, and w denote the zonal and meridional components of horizontal wind and the vertical velocity, respectively. θ, a, f, z, ϕ, ρ, and p represent the potential temperature, Earth radius, Coriolis parameter, geopotential height, latitude, air density, and air pressure. The overbar, prime, and asterisk denote zonal mean, departure from zonal mean and residual circulation, respectively. The residual stream function $\overline{\chi}^*$ is calculated based on the following two equations:

$$\rho\overline{v}^* = -\frac{\partial\overline{\chi}^*}{\partial z} \tag{6}$$

$$\rho\overline{w}^* = \frac{\partial\overline{\chi}^*}{\partial y} \tag{7}$$

All these quantities are calculated based on daily data for both ERA-5 reanalysis and WACCM simulations. The relationship between the residual stream function and the vertical gradient of E-P flux divergence can be interpreted using the following equation[51]:

$$\frac{\partial^2\overline{\chi}^*}{\partial y^2} + \rho\frac{f^2}{N^2}\frac{\partial}{\partial z}\left(\frac{1}{\rho}\frac{\partial\overline{\chi}^*}{\partial z}\right) = \frac{\rho}{N^2}\left[\frac{\partial}{\partial y}\left(\frac{k\overline{J}}{H}\right) + f\frac{\partial\overline{G}}{\partial z}\right] \tag{8}$$

where

$$N^2 \equiv \frac{R}{H}\left(\frac{kT}{H} + \frac{dT}{dz}\right) \tag{9}$$

where k, J, N, G, R, H, and T denote ratio of gas constant to specific heat, diabatic heating rate, Brunt-Vaisala frequency (Eq. 9), zonal wave drag due to eddies, gas constant for dry air, scale height, and air temperature. Considering the elliptic operator on the left hand side of Eq. 8 is approximately proportional to $-\overline{\chi}^*$, there is an inverse proportional relation between the residual stream function and the vertical gradient of wave divergence.

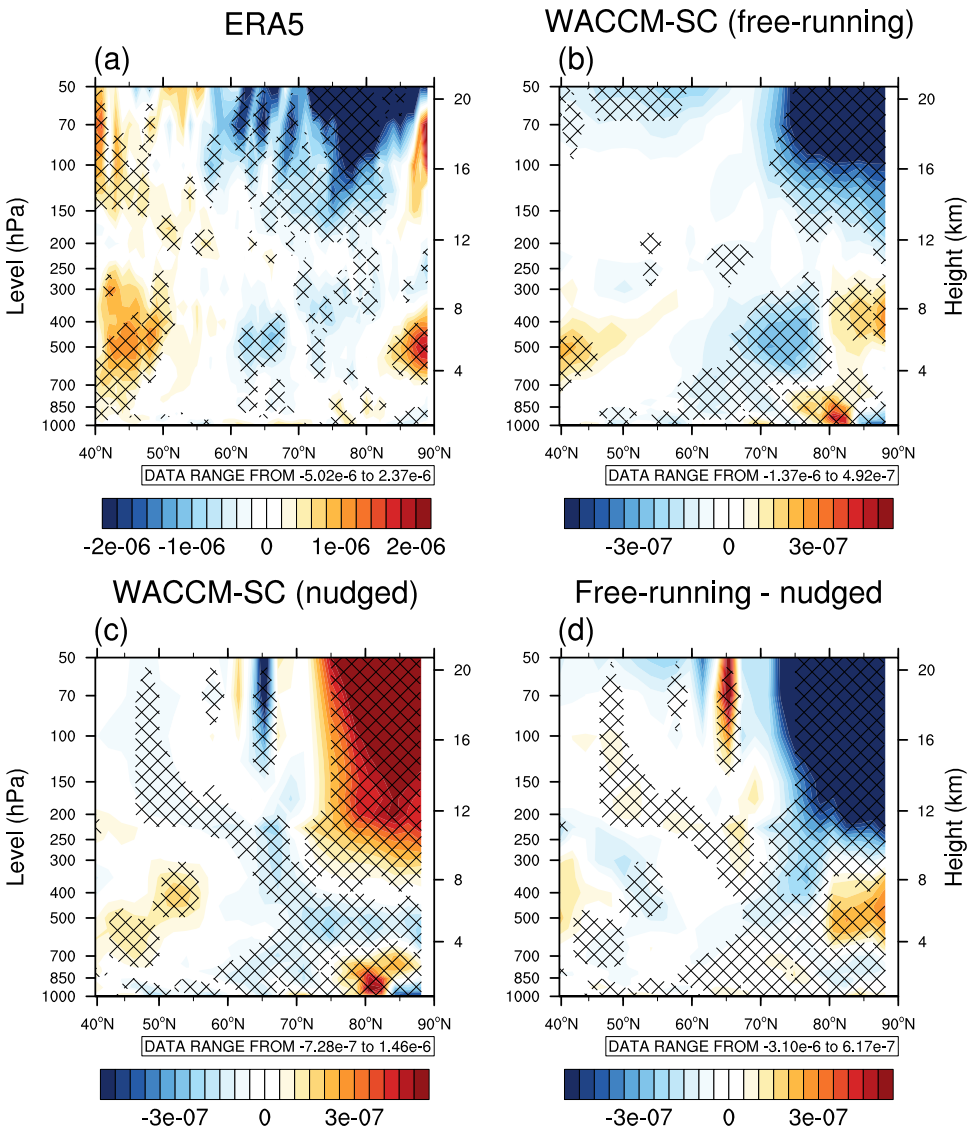

Fig. 4 Winter residual vertical velocity anomalies induced by BKS sea-ice loss. a Winter-mean residual vertical velocity (m s^{-1}; scaled by air pressure) regressed against BKS sea ice, multiplied by the composited SIC differences between BKS low- and high-SIC years, derived from the ERA5 reanalysis. Simulated differences of zonal-mean winter residual vertical velocity between LICE and HICE runs in the **b** free-running WACCM-SC simulations, **c** nudged WACCM-SC simulations, and **d** their differences (free-running minus nudged). The information of data range is placed above label bar. Hatched regions are statistically significant at the 90% confidence level according to bootstrap resampling statistical test.

The temperature tendency of the Arctic mid-to-upper troposphere is diagnosed using the TEM temperature tendency equation[51]:

$$\frac{\partial \overline{T}}{\partial z} = -N^2 \frac{H}{R}\overline{w}^* + \frac{\overline{J}}{C_p} \tag{10}$$

where C_p denotes the specific heat capacity, respectively. The term on the left hand side of Eq. 10 is zonal-mean temperature tendency and the two terms on the right hand side denote zonal-mean temperature tendency due to adiabatic heating/cooling induced by vertical motion and diabatic processes, respectively. The temperature tendency of the Arctic mid-to-upper troposphere contributed by adiabatic process due to vertical motion is calculated on each grid first and then averaged between 600 and 225 hPa (225 hPa is the first pressure level below the nudging region), north of 65°N, based on daily data for both ERA-5 reanalysis and WACCM simulations.

Bootstrap resampling[57] is applied in this study to test whether the composite analysis is statistically significant. Assume there are two samples, X_1 and X_2, with sample sizes N_1 and N_2, respectively. We resample randomly the subsets, with sample sizes n_1 and n_2 ($n_1 \le N_1$, $n_2 \le N_2$) respectively, from the two samples for 1000 times and calculate the differences. Then, 95th and 5th percentiles of this 1000-time resampling are calculated as the upper and lower thresholds of the 90% confidence level. The two samples could be regarded as statistically significantly different from each other at 90% confidence level, if zero is excluded from the above-mentioned confidence interval. And vice versa if zero is included in that confidence interval.

WACCM-SC simulations

We conducted bespoke simulations with the specified chemistry version of the Whole Atmosphere Community Climate Model with

4.0 (WACCM-SC). More details on the model Smith et al.[58]. Four experiments were performed in this study, a pair of free-running simulations and a pair of simulations with the stratosphere nudged to climatological state, derived from an extra control experiment prescribed with climatological SIC condition during 1982–2001 (CTRL). Both pairs of experiments consist of a run prescribed with anomalously high BKS SIC condition (HICE and HICE_ndg) and a run with anomalously low BKS SIC condition (LICE and LICE_ndg).

The boundary conditions for BKS high- and low-SIC runs are derived from composites of BKS low- and high-SIC years selected from HadISST1 dataset during 1979–2016, using the same method described in the previous section. According to these selection criteria, 7 years were selected with high BKS SIC (1988, 1997, 1998, 2002, 2003, 2010, and 2014) and 3 years with low BKS SIC (1984, 2012, and 2016) (Supplementary Fig. 6a). The composited BKS high- and low-SIC conditions are prescribed throughout the whole seasonal cycle in the simulations. The composited differences of early winter SST/SIC conditions between the selected BKS low- and high-SIC years are shown in Supplementary Figs. 7a, b. Also, the corresponding SST condition is applied where SIC condition is changed, whereas SST condition in the remaining area is the climatology of 1982–2001. The differences of early winter SST/SIC boundary conditions applied for the BKS low- and high-SIC runs are shown in Supplementary Fig. 7c, d. The SST/SIC condition of CTRL run is fixed as the climatological seasonal cycle during 1982–2001. Apart from the SIC and SST conditions, all the experiments are forced by the same initial conditions and repeating seasonal cycle of boundary conditions. All these experiments are integrated for 210 years, with the first 3 years discarded as the model spin-up.

Stratospheric nudging

The nudging technique is similar to that used in Zhang et al.[39,40], Labe et al.[20], and Xu et al.[41,42], and is performed according to the following steps. First, we ran a control experiment (hereafter CTRL) driven by the climatological forcing to get a climatological seasonal cycle of the atmospheric state. This climatological state is then used as the reference profile for the HICE_ndg and LICE_ndg runs. Second, we selected the polar stratosphere (above 100 hPa, north of 66°N) as the nudging region and applied a mask coefficient, which determined the nudging strength, with 1 denoting full-strength nudge and 0 where no nudging is applied. This coefficient was set to 1 above 100 hPa and north of 66 °N, and gradually decreased to 0 from 100 to 200 hPa vertically, and from 66 to 60 °N meridionally, in order to avoid abrupt changes. Elsewhere, the coefficient is set to 0. Finally, the horizontal wind and air temperature fields in the HICE_ndg and LICE_ndg runs were nudged toward the climatological state mentioned every 3 model hours. It should be noted that we assume that the effect of nudging is independent of sea-ice state and hence the influence of nudging is removed when calculating the differences between the two nudged experiments.

PAMIP multi-model ensemble

Two experiments are analyzed in this study: pdSST-pdSIC and pdSST-futBKSeasSIC. The experiment pdSST-pdSIC was prescribed with the 1979–2008 climatology of SST/SIC conditions from HadISST. The pdSST- futBKSeasSIC experiment was forced by the same SST/SIC conditions except for the BKS region, where the SIC condition is substituted values representative of the future at the time of 2 K warming above preindustrial levels. The differences of SST/SIC conditions between pdSST-futBKSeasSIC and pdSST-pdSIC are shown in Supplementary Fig. 7e, f. 1200 ensemble members from eight models in total are used (Supplementary Table 1). Considering the differences of sea-ice forcing between PAMIP project and WACCM simulations (also reanalysis), all the PAMIP results have been multiplied by the ratio of the observed BKS SIC index differences between low-SIC and high-SIC years against the PAMIP forcing (1.16 after calculation), for a better comparison with reanalysis and WACCM results. Moreover, it should be noted that not all variables or daily outputs used for the analysis are available in PAMIP. Therefore, only the results of air temperature and zonal wind are shown in this study.

DATA AVAILABILITY

The atmospheric variables (1979–2021) are from ERA-5 reanalysis dataset provided by the European Center for Medium-Range Weather Forecasts (ECMWF)[59]. The horizontal resolution is 1° × 1° and there are 37 vertical levels ranging from 1000 to 1 hPa. Monthly mean sea surface temperature (SST) and sea ice concentration (SIC) with a horizontal resolution of 1° × 1° are from Hadley Center Sea Ice and Sea Surface Temperature dataset (HadISST1)[60]. Multi-model large-ensemble experiment data from the Polar Amplification Model Intercomparison Project (PAMIP)[61] contribution to the sixth Coupled Model Intercomparison Project (CMIP6)[62] are available on https://esgf-index1.ceda.ac.uk/search/cmip6-ceda/.

CODE AVAILABILITY

All codes are available on request by contacting the corresponding author (wstian@lzu.edu.cn).

Received: 23 February 2022; Accepted: 8 February 2023;
Published online: 20 February 2023

REFERENCES

1. Cohen, J. et al. Recent Arctic amplification and extreme mid-latitude weather. *Nat. Geosci.* **7**, 627–637 (2014).
2. England, M. R., Eisenman, I., Lutsko, N. J. & Wagner, T. J. The recent emergence of Arctic amplification. *Geophys. Res. Lett.* **48**, 15 (2021).
3. Screen, J. A. & Simmonds, I. The central role of diminishing sea ice in recent Arctic temperature amplification. *Nature* **464**, 1334–1337 (2010).
4. Serreze, M. C. & Francis, J. A. The arctic amplification debate. *Clim. Change* **76**, 241–264 (2006).
5. Coumou, D., Capua, G. D., Vavrus, S., Wang, L. & Wang, S. The influence of Arctic amplification on mid-latitude summer circulation. *Nat. Commun.* **9**, 2959 (2018).
6. Francis, J. A. & Vavrus, S. J. Evidence linking Arctic amplification to extreme weather in mid-latitudes. *Geophys. Res. Lett.* https://doi.org/10.1029/2012GL051000 (2012).
7. Screen, J. A. & Simmonds, I. Exploring links between Arctic amplification and mid-latitude weather. *Geophys. Res. Lett.* **40**, 959–964 (2013).
8. Vavrus, S. J. The influence of Arctic amplification on mid-latitude weather and climate. *Curr. Clim. Change Rep.* **4**, 238–249 (2018).
9. Wu, Y. T. & Smith, K. L. Response of Northern Hemisphere midlatitude circulation to Arctic amplification in a simple atmospheric general circulation model. *J. Clim.* **29**, 2041–2058 (2016).
10. Cohen, J. et al. Divergent consensuses on Arctic amplification influence on midlatitude severe winter weather. *Nat. Clim. Change* **10**, 20–29 (2020).
11. Dai, A. & Song, M. Little influence of Arctic amplification on mid-latitude climate. *Nat. Clim. Change* **10**, 231–237 (2020).
12. Overland, J. E. & Wang, M. Large-scale atmospheric circulation changes are associated with the recent loss of Arctic sea ice. *Tellus A* **62**, 1–9 (2010).
13. Sellevold, R., Sobolowski, S. & Li, C. Investigating possible Arctic–midlatitude teleconnections in a linear framework. *J. Clim.* **29**, 7329–7343 (2016).
14. He, S., Xu, X., Furevik, T. & Gao, Y. Eurasian cooling linked to the vertical distribution of Arctic warming. *Geophys. Res. Lett.* **47**, e2020GL087212 (2020).
15. Xu, X. et al. Contributors to linkage between Arctic warming and East Asian winter climate. *Clim. Dyn.* **57**, 2543–2555 (2021).
16. Zhang, R. N., Zhang, R. H. & Sun, C. Modulation of the interdecadal variation of atmospheric background flow on the recent recovery of the EAWM during the 2000s and its link with North Atlantic–Arctic warming. *Clim. Dyn.* **59**, 561–578 (2022).
17. Mori, M., Watanabe, M., Shiogama, H., Inoue, J. & Kimoto, M. Robust Arctic sea-ice influence on the frequent Eurasian cold winters in past decades. *Nat. Geosci.* **7**, 869–873 (2014).
18. Mori, M., Kosaka, Y., Watanabe, M., Nakamura, H. & Kimoto, M. A reconciled estimate of the influence of Arctic sea-ice loss on recent Eurasian cooling. *Nat. Clim. Change* **9**, 123–129 (2019).

19. Overland, J. E., Wood, K. R. & Wang, M. Warm Arctic-cold continents: climate impacts of the newly open Arctic Sea. *Polar Res.* https://doi.org/10.3402/polar.v30i0.15787 (2011).
20. Labe, Z., Peings, Y. & Magnusdottir, G. Warm arctic, cold Siberia pattern: role of full arctic amplification versus sea ice loss alone. *Geophys. Res. Lett.* **47**, e2020GL088583 (2020).
21. Kumar, A. et al. Contribution of sea ice loss to Arctic amplification. *Geophys. Res. Lett.* https://doi.org/10.1029/2010GL045022 (2010).
22. Overland, J. E. et al. The recent shift in early summer Arctic atmospheric circulation. *Geophys. Res. Lett.* https://doi.org/10.1029/2012GL053268 (2012).
23. Pistone, K., Eisenman, I. & Ramanathan, V. Observational determination of albedo decrease caused by vanishing Arctic sea ice. *Proc. Natl Acad. Sci. USA* **111**, 3322–3326 (2014).
24. Stuecker, M. F. et al. Polar amplification dominated by local forcing and feedbacks. *Nat. Clim. Change* **8**, 1076–1081 (2018).
25. Wendisch, M. et al. The Arctic cloud puzzle: using ACLOUD/PASCAL multiplatform observations to unravel the role of clouds and aerosol particles in Arctic amplification. *Bull. Am. Meteorol. Soc.* **100**, 841–871 (2019).
26. Previdi, M. et al. Arctic amplification: a rapid response to radiative forcing. *Geophys. Res. Lett.* **47**, e2020GL089933 (2020).
27. Boeke, R. C., Taylor, P. C. & Sejas, S. A. On the nature of the Arctic's positive lapse-rate feedback. *Geophys. Res. Lett.* **48**, e2020GL091109 (2021).
28. Hwang, Y. T., Frierson, D. M. W. & Kay, J. E. Coupling between Arctic feedbacks and changes in poleward energy transport. *Geophys. Res. Lett.* https://doi.org/10.1029/2011GL048546 (2011).
29. Screen, J. A., Deser, C. & Simmonds, I. Local and remote controls on observed Arctic warming. *Geophys. Res. Lett.* **39**, 10709 (2012).
30. Zhang, X. et al. Enhanced poleward moisture transport and amplified northern high-latitude wetting trend. *Nat. Clim. Change* **3**, 47–51 (2013).
31. Screen, J. A. & Francis, J. A. Contribution of sea-ice loss to Arctic amplification is regulated by Pacific Ocean decadal variability. *Nat. Clim. Change* **6**, 856 (2016).
32. Deser, C., Tomas, R. A. & Sun, L. The role of ocean–atmosphere coupling in the zonal-mean atmospheric response to Arctic sea ice loss. *J. Clim.* **28**, 2168–2186 (2015).
33. Sun, L., Deser, C. & Tomas, R. A. Mechanisms of stratospheric and tropospheric circulation response to projected Arctic sea ice loss. *J. Clim.* **28**, 7824–7845 (2015).
34. Screen, J. A. Simulated atmospheric response to regional and pan-Arctic sea ice loss. *J. Clim.* **30**, 3945–3962 (2017).
35. McKenna, C. M., Bracegirdle, T. J., Shuckburgh, E. F., Haynes, P. H. & Joshi, M. M. Arctic sea ice loss in different regions leads to contrasting Northern Hemisphere impacts. *Geophys. Res. Lett.* **45**, 945–954 (2018).
36. Kim, B. M. et al. Weakening of the stratospheric polar vortex by Arctic sea-ice loss. *Nat. Commun.* **5**, 1–8 (2014).
37. Nakamura, T. et al. The stratospheric pathway for Arctic impacts on midlatitude climate. *Geophys. Res. Lett.* **43**, 3494–3501 (2016).
38. Zhang, J. K., Tian, W. S., Chipperfield, M. P., Xie, F. & Huang, J. L. Persistent shift of the Arctic polar vortex towards the Eurasian continent in recent decades. *Nat. Clim. Change* **6**, 1094 (2016).
39. Zhang, P. F. et al. A stratospheric pathway linking a colder Siberia to Barents-Kara Sea sea ice loss. *Sci. Adv.* **4**, eaat6025 (2018).
40. Zhang, J. K. et al. Impacts of stratospheric polar vortex changes on wintertime precipitation over the northern hemisphere. *Clim. Dynam.* **58**, 3155–3171 (2022).
41. Xu, M., Tian, W., Zhang, J., Wang, T. & Qie, K. Impact of Barents-Kara-Sea sea ice reduction on the variation of east Asian trough in late winter. *J. Climate* https://doi.org/10.1175/JCLI-D-20-0205.1 (2020).
42. Xu, M. et al. Distinct tropospheric and stratospheric mechanisms linking historical Barents-Kara Sea-Ice ioss and late winter Eurasian temperature variability. *Geophys. Res. Lett.* **48**, 20 (2021).
43. Cohen, J., Agel, L., Barlow, M., Garfinkel, C. I. & White, I. Linking Arctic variability and change with extreme winter weather in the United States. *Science* **373**, 1116–1121 (2021).
44. Zhang, R. N., Zhang, R. H. & Dai, G. Intraseasonal contributions of Arctic sea-ice loss and Pacific decadal oscillation to a century cold event during early 2020/21 winter. *Clim. Dyn.* **58**, 741–758 (2021).
45. Screen, J. A. et al. Atmospheric impacts of Arctic sea-ice loss, 1979–2009: separating forced change from atmospheric internal variability. *Clim. Dynam.* **43**, 333–344 (2014).
46. Peings, Y., Labe, Z. M. & Magnusdottir, G. Are 100 ensemble members enough to capture the remote atmospheric response to+ 2 °C Arctic sea ice loss? *J. Clim.* **34**, 3751–3769 (2021).
47. Siew, P. Y. F., Li, C., Sobolowski, S. P. & King, M. P. Intermittency of Arctic–mid-latitude teleconnections: stratospheric pathway between autumn sea ice and the winter North Atlantic Oscillation. *Weather Clim. Dynam.* **1**, 261–275 (2020).
48. Smith, D. M. et al. Robust but weak winter atmospheric circulation response to future Arctic sea ice loss. *Nat. Comm.* **13**, 1–15 (2022).
49. Deser, C., Tomas, R., Alexander, M. & Lawrence, D. The seasonal atmospheric response to projected Arctic sea ice loss in the late twenty-first century. *J. Clim.* **23**, 333–351 (2010).
50. Graversen, R. G., Mauritsen, T., Tjernström, M., Källén, E. & Svensson, G. Vertical structure of recent Arctic warming. *Nature* **451**, 53–56 (2008).
51. Holton, J. R. *An Introduction to Dynamic Meteorology* 4th edn 535 (Elsevier, 2004).
52. Bloxam, K. & Huang, Y. Radiative and dynamic contributions to the observed temperature trends in the Arctic winter atmosphere. *Clim. Dynam.* **60**, 257–277 (2022).
53. Randel, W. & Held, I. Phase speed spectra of transient eddy fluxes and critical layer absorption. *J. Atmos. Sci.* **48**, 688–697 (1991).
54. Chen, G. & Held, I. M. Phase speed spectra and the recent poleward shift of Southern Hemisphere surface westerlies. *Geophys. Res. Lett.* https://doi.org/10.1029/2007GL031200 (2007).
55. Schubert, S. et al. An atlas of ECMWF analyses (1980–87). Part 1: First momet quantities. *NASA Tech. Memo*. 100747 (1990).
56. Andrews, D. G., Holton, J. R. & Leovy, C. B. *Middle Atmosphere Dynamics* 489 (Academic Press Inc, 1987).
57. Gilleland, E. Bootstrap methods for statistical inference. Part I: Comparative forecast verification for continuous variables. *J. Atmos. Ocean. Tech.* **37**, 2117–2134 (2020).
58. Smith, K. L., Neely, R. R., Marsh, D. R. & Polvani, L. M. The specified chemistry whole atmosphere community climate model (SC-WACCM). *J. Adv. Model. Earth Syst.* **6**, 883–901 (2014).
59. Hersbach, H. B. et al. The ERA5 global reanalysis. *Quart. J. R. Meteor. Soc.* **146**, 1999–2049 (2020).
60. Rayner, N. A. A. et al. Global analyses of sea surface temperature, sea ice, and night marine air temperature since the late nineteenth century. *J. Geophys. Res.* https://doi.org/10.1029/2002JD002670 (2003).
61. Smith, D. M. et al. The Polar Amplification Model Intercomparison Project (PAMIP) contribution to CMIP6: investigating the causes and consequences of polar amplification. *Geosci. Model Dev.* **12**, 1139–1164 (2019).
62. Eyring, V. et al. Overview of the Coupled Model Intercomparison Project Phase 6 (CMIP6) experimental design and organization. *Geosci. Model Dev.* **9**, 1937–1958 (2016).

ACKNOWLEDGEMENTS

This research was supported by the National Natural Science Foundation of China (42130601, 42075062), the Fundamental Research Funds for the Central Universities (lzujbky-2021-ey04) and ArctiCONNECT (NERC grant NE/V005855/1). We thank Doug Smith for providing valuable comments on the manuscript and thank Javier Garcia-Serrano, Rym Msadek, Yannick Peings, Rosie Eade, Tido Semmler, and Lantao Sun for sharing PAMIP simulations prior to their release on the Earth System Grid.

AUTHOR CONTRIBUTIONS

M.X., W.S.T., and J.K.Z. designed the project. M.X. performed model experiments and data analysis. J.A.S. interpreted the data and results and revised the manuscript. Z.W. and C.Y.Z. calculated some diagnostics used in this study. All authors contributed to the writing of the paper.

COMPETING INTERESTS

The authors declare no competing interests.

ADDITIONAL INFORMATION

Supplementary information The online version contains supplementary material available at https://doi.org/10.1038/s41612-023-00333-2.

Correspondence and requests for materials should be addressed to Wenshou Tian or Jiankai Zhang.

Reprints and permission information is available at http://www.nature.com/reprints

Publisher's note Springer Nature remains neutral with regard to jurisdictional claims in published maps and institutional affiliations.

Open Access This article is licensed under a Creative Commons Attribution 4.0 International License, which permits use, sharing, adaptation, distribution and reproduction in any medium or format, as long as you give appropriate credit to the original author(s) and the source, provide a link to the Creative Commons license, and indicate if changes were made. The images or other third party material in this article are included in the article's Creative Commons license, unless indicated otherwise in a credit line to the material. If material is not included in the article's Creative Commons license and your intended use is not permitted by statutory regulation or exceeds the permitted use, you will need to obtain permission directly from the copyright holder. To view a copy of this license, visit http://creativecommons.org/licenses/by/4.0/.

© The Author(s) 2023